ChemEurJ

Research Article
doi.org/10.1002/chem.202502472

Chemistry Europe
European Chemical Societies Publishing

www.chemeurj.org

Targeting G-Rich lncRNA and Its Structural Polymorphism With Selective G-Quadruplex Ligands: An NMR Study

Giuseppe Satta,[a, b] Jasna Brčić,[a] and Janez Plavec*[a, c, d]

Long noncoding RNAs (lncRNAs) play essential regulatory roles, often mediated by complex structural elements such as RNA G-quadruplexes (rGQs). While ligand interactions with DNA G-quadruplexes (dGQs) have been extensively studied, for rGQs remain less explored. Here, we studied the SL15P RNA oligonucleotide derived from the REG1CP lncRNA, which adopts a parallel rGQ structure in equilibrium with a hairpin (Hp). A set of 12 small molecules, previously known for their ability to make complex with dGQs, was tested for their ability to bind and stabilize the SL15P rGQ. Using NMR spectroscopy, we analyzed complex formation and assessed whether these ligands could promote rGQ folding under conditions where the Hp structure is favored. Melting experiments with circular dichroism (CD) quantified the thermal stabilization induced by ligand binding. Our results show that ligands known to target dGQs exhibit different behaviors toward rGQs. Among the tested compounds, 360A, PhenDC3, and PDS proved to be the most effective, as they induced well-defined complex formation and significant stabilization of the SL15P rGQ. PhenDC3 showed evidence of a dual binding interaction. This study emphasizes that the binding of ligands to rGQs can be highly variable and supports the rational design of selective compounds for therapeutic purposes.

1. Introduction

Long noncoding RNAs (lncRNAs) play key roles in gene expression regulation, chromatin organization, and RNA metabolism.[1–12] Although initially considered as transcriptional noise due to their low sequence conservation and expression levels, they are now recognized as functional molecules involved in both physiological and pathological processes.[13,14] A notable characteristic of many lncRNAs is their ability to fold into complex secondary and tertiary structures, facilitating specific interactions with proteins, nucleic acids, and small molecules.[15] It is widely accepted that RNA functions are primarily determined by its 3D conformation rather than its linear nucleotide sequence; thus, precise characterization of RNA structure is crucial for elucidating its diverse functional mechanisms and regulatory roles.[16,17] RNA can assume a broad array of structural motifs, including hairpin (Hp), bulge and inner loop, three-way junction, kissing loop, pseudoknot, and G-quadruplex (rGQ).[18] Among these, rGQs have garnered particular interest. GQs are stable four-stranded noncanonical structures formed by guanine-rich sequences that fold into planar G-quartets, stabilized by Hoogsteen hydrogen bonds and monovalent cations, such as sodium or potassium.[19] From a structural point of view, DNA and RNA G-quadruplexes (rGQs) share the same fundamental architecture. However, the presence of the 2′-hydroxyl group in RNA affects the hydration and intermolecular interaction network, often resulting in a higher thermodynamic stability of rGQs compared to their DNA counterparts.[20] Additionally, the 2′-hydroxyl group imposes conformational constraints that favor the anti-glycosidic torsion angle and influence sugar puckering, resulting in rGQs predominantly adopting parallel-folding topologies.[21,22] Putative GQ sequences have been identified extensively throughout the human transcriptome, including many lncRNAs.[23] Several studies have demonstrated that rGQs within lncRNAs play crucial regulatory roles due to their ability to mediate specific molecular interactions.[24] In MALAT1, rGQ facilitates binding to nucleolin and nucleophosmin, thereby modulating nuclear architecture and transcriptional output.[25] Similarly, GSEC lncRNA forms GQs that interact with DHX36 helicase, affecting cell motility in colorectal cancer.[26] These findings support the broader perspective of rGQs as regulatory scaffolds that integrate sequences and structures to control gene expression. In this study, we focused on the rGQ-forming sequence within REG1CP lncRNA, which plays a regulatory role in REG3A transcription. Specifically, REG1CP is upregulated in colorectal cancer and modulates REG3A gene expression through a

[a] Dr. G. Satta, Dr. J. Brčić, Prof. Dr. J. Plavec
Slovenian NMR Centre, National Institute of Chemistry, Ljubljana SI-1000, Slovenia
E-mail: janez.plavec@ki.si

[b] Dr. G. Satta
CERIC-ERIC, S.S. 14 - Km 163,5 in AREA Science Park, Trieste (Basovizza) 34149, Italy

[c] Prof. Dr. J. Plavec
EN→FIST Centre of Excellence, Trg OF 13, Ljubljana SI-1000, Slovenia

[d] Prof. Dr. J. Plavec
Faculty of Chemistry and Chemical Technology, University of Ljubljana, Vecna pot 113, Ljubljana SI-1000, Slovenia

This paper is dedicated to the memory of the late Prof. Frank Seela, whose pioneering contributions to nucleic acid chemistry continue to inspire.

Supporting information for this article is available on the WWW under https://doi.org/10.1002/chem.202502472

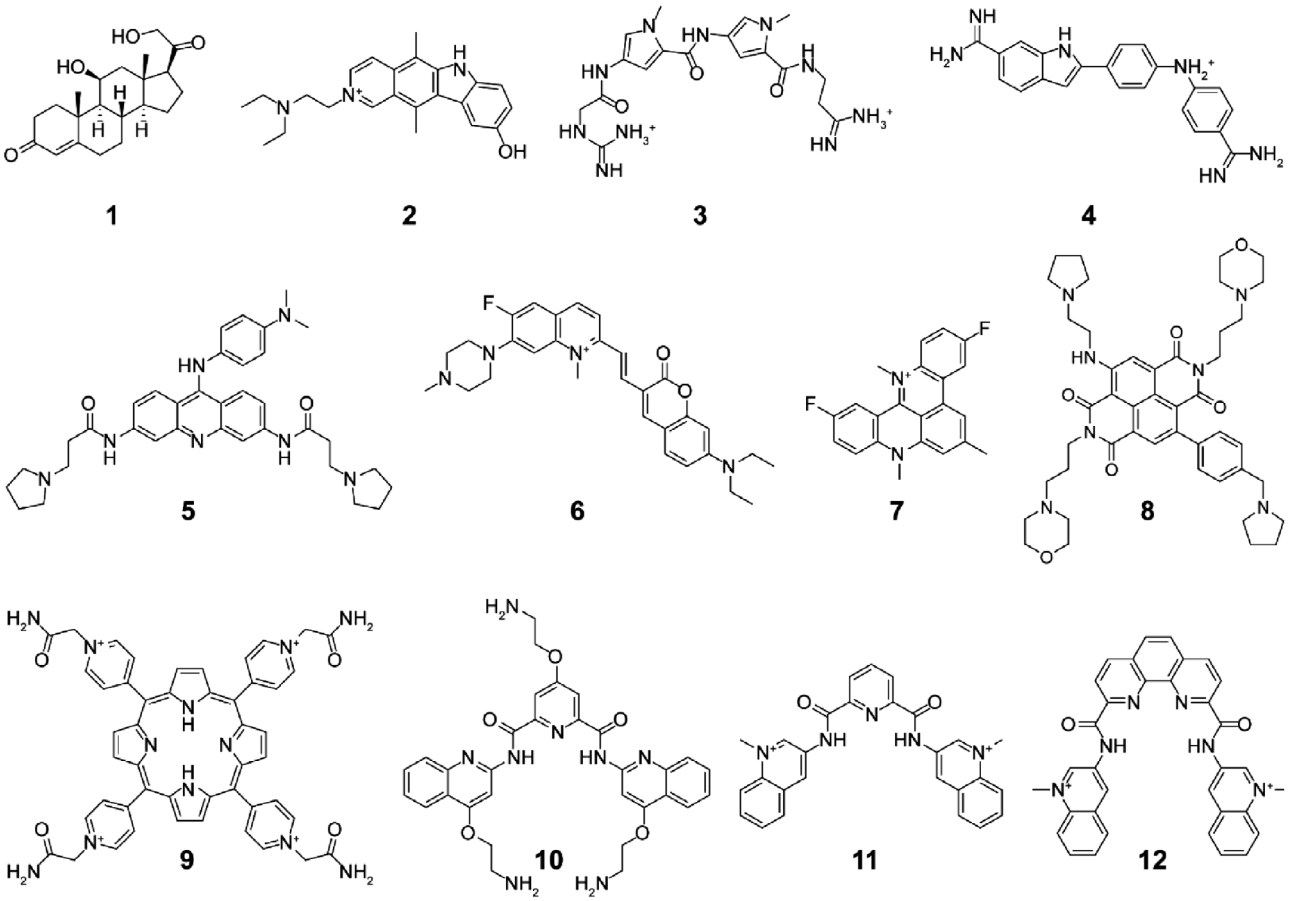

Figure 1. Chemical structure of small molecules (the respective salt forms were used) selected for the screening of binding to SL15P rGQ: Corticosterone (1), Datelliptium (2), Netropsin (3), Synucleozide (4), BRACO-19 (5), QUMA-1 (6), RHSP4 (7), SOP1812 (8), PL7 (9), PDS (10), 360A (11), and PhenDC3 (12).

Table 1. RNA oligonucleotides employed for structural and binding analyses in this study.

	1	2	3	4	5	6	7	8	9	10	11	12	13	14	15	16	17	18	19	20	21	22	23	24	25	26	27	28	29	30
SL15P[a]	U	G	U	**G**	**G**	**G**	A	A	**G**	**G**	**G**	A	G	G	C	U	C	A	C	G	A	A	**G**	**G**	**G**	A	**G**	**G**	**G**	G
SL15PU15	U	G	U	**G**	**G**	**G**	A	A	**G**	**G**	**G**	A	G	G	U	U	C	A	C	G	A	A	**G**	**G**	**G**	A	**G**	**G**	**G**	G

[a]Wild type.

two-step structural mechanism. At one end of the chain, it forms an RNA–DNA triplex with the distal promoter of REG3A, while at the other end, it folds into a GQ that recruits the FANCJ DNA helicase.[27] The REG1CP-REG3A-FANCJ axis promotes chromatin remodeling and enables GRα-mediated transcriptional activation of REG3A, leading to increased proliferation and tumorigenicity in colorectal cancer cells.[27] It appears that the putative rGQ-forming site within REG1CP is necessary for its interaction with FANCJ. Here we report a 30-nt guanine-rich RNA oligoribonucleotide containing the rGQ-forming site of REG1CP,[28] referred to as SL15P in the present study. Our study focused on the interaction of the SL15P rGQ with small molecules known for their ability to bind and stabilize GQ structures. We hypothesize that formation of a stable complex may interfere in the interaction between REG1CP and FANCJ, thereby inhibiting its recruitment activity and consequently modulating the transcriptional activation pathway.[29] We conducted a screening of a small library of molecules with different structures and functionalities to evaluate their ability to form complexes with rGQ. Understanding these interactions provides a basis for investigating how such complexes modulate RNA structure and influence RNA-related functions.

Although thousands of GQ-selective ligands have been reported, the majority of them have been designed for targeting DNA GQs (dGQs), with applications ranging from anticancer strategies to molecular probes.[30] Except for a few of them, the selectivity and binding ability toward GQs formed by RNA sequences, specifically those from lncRNAs, remain to be explored. A group of twelve ligands (Figure 1) was selected for this study based on their previously reported binding modes to nucleic acid secondary structures (Table 1). The small library included well-characterized G-quartet stacking ligands as well as

Table 2. Molecular scaffolds of the tested compounds and their expected interaction modes with GQ structures.

#	Ligand[a]	Scaffold	Binding mode[b]
1	Corticosterone	Polycyclic	Short Loop Binding
2	Datelliptium	Ellipticine	Long/Short Loop Binding
3	Netropsin	Poly pyrroles	Long/Short Loop Binding
4	Synucleozide	Indole	Long/Short Loop Binding
5	BRACO-19	Acridine	Stacking
6	QUMA-1	Coumarin	Stacking
7	RHSP4	Polycyclic Acridine	Stacking
8	SOP1812	Naphthalene Diimide	Stacking
9	PL7	Porphyrin	Stacking
10	PDS	2,6-pyridine-dicarboxamide	Stacking
11	360A	2,6-pyridine-dicarboxamide	Stacking
12	PhenDC3	Phenanthroline	Stacking/Intercalation

[a]Most ligands are commercially available, except for PL7, a generous gift from Prof. M. Carraro.[40]
[b]The color codes correspond to those in Figure 2.

compounds known to interact with alternative GQ moieties or to destabilize their structure. For example, corticosterone (**1**) was chosen due to its ability to stabilize Hp structures while destabilizing GQ.[31] Datelliptium (**2**) is a selective binder of expanded r(CGG) repeats known to disrupt toxic RNA–protein aggregates associated with fragile X-associated tremor/ataxia syndrome.[32] Netropsin (**3**) is a polyamide with antibiotic and antiviral activity reported in literature as GQ grooves binder,[33] while Synucleozide (**4**), an indole derivative, was shown to interact with the Hp of mRNA, inhibiting its unwinding and subsequent incorporation into polysomes, thereby reducing α-synuclein translation.[34] Our screening also included well-studied GQ-binding ligands, such as BRACO-19 (**5**), an acridine-based ligand that interacts with G-quartets via π–π stacking and further stabilizes the complex through groove binding via its tertiary amine side chains.[35,36] QUMA-1 (**6**), developed in 2018, is a highly selective "turn-on" fluorescent probe for rGQs. Under in vitro conditions and in living cells, it fluoresces only upon binding to rGQs, allowing real-time monitoring of their folding and unfolding, as well as helicase activity.[37] RHSP4 (**7**), a pentacyclic quinoacridinium derivative first described in 2001, was included due to its high telomerase inhibitory activity and its ability to stabilize dGQs.[38] SOP1812 (**8**), a tetrasubstituted naphthalene diimide derivative developed in 2020, was selected for its promising pharmacological profile, improved cellular activity compared to previous analogues, and nanomolar affinity for human GQs.[39] Based on previous studies, PL7 (**9**), a porphyrin derivative, was selected for its ability to bind to both parallel and hybrid dGQs.[40] Two derivatives of 2,6-pyridinedicarboxamide, PDS (**10**) and 360A (**11**), originally developed to inhibit telomerase by stabilizing telomeric dGQs, were also included.[41,42] PhenDC3 (**12**), a phenanthroline-based ligand,[43] is known for both stacking on G-quartets and intercalation into specific dGQ topologies. PhenDC3 (**12**) can induce a conformational change from a hybrid to an antiparallel chair-type in human telomeric dGQ by displacing a potassium ion upon intercalation.[44]

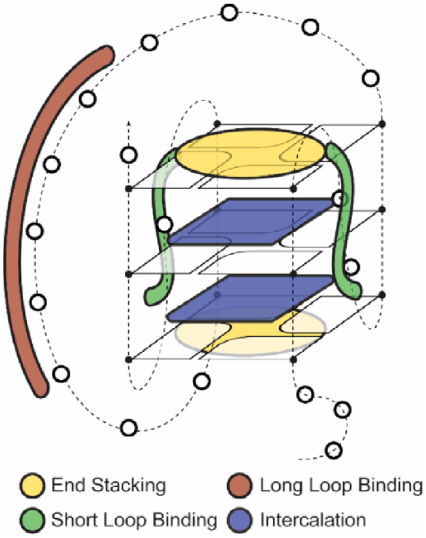

Figure 2. Schematic illustration of expected ligand interaction modes.

Ligand screenings targeting rGQs reported in the literature are predominantly based on computational approaches.[45,46] To date, not many NMR-monitored ligand interaction studies on rGQs have been reported. One of them is the study by Garavis et al., which investigated fluorinated ligands for TERRA rGQ using ^{19}F-NMR techniques.[47] To the best of our knowledge, no systematic screening of small-molecule binding to lncRNA-derived rGQs has been reported. Therefore, we considered it worthwhile to investigate this aspect via NMR spectroscopy. An initial screening was performed by titrating SL15P sequence with each of the 12 ligands and recording 1D ^{1}H spectra at each titration step. This approach provided evidence of ligand interaction with the rGQ structure and subsequent complex formation (Table 2, Figure 2).

From titrations, five ligands that induced the appearance of distinct new sets of imino-proton resonances, diagnostic of

complex formation, were selected for further analysis of their ability to refold the oligonucleotide into the rGQ structure, starting from an Hp-dominated state. This part of the study aimed to determine whether ligand binding could influence the folding pathway of SL15P, thereby promoting the formation of a ligand-induced rGQ structure that may be distinct from the one naturally adopted by the oligonucleotide. The same selected ligands were then tested for their ability to thermally stabilize the rGQ using circular dichroism (CD) melting experiments. These were conducted on a mutant sequence that was designed to fold exclusively into the rGQ structure. The presence in solution of a second structure, such as a Hp, would influence the melting temperature of the target species, thereby providing nonspecific results for the complex. The results highlight the efficiency of selected ligands, especially PDS (**10**) and PhenDC3 (**12**), in promoting the formation of specific rGQ–ligand complexes and improving thermal stability. Some ligands prevented the unfolding of rGQ even at temperatures close to 100 °C, indicating the formation of exceptionally stable complexes.

2. Results and Discussion

2.1. NMR Evidence for Structural Equilibrium in the SL15P Sequence

In NMR study of noncanonical nucleic acid structures, the most informative region of the spectrum is the imino proton region (δ 10-15 ppm), which directly gives evidence of base pairing. Watson-Crick base pairs typically show resonances between δ 12-15 ppm, whereas Hoogsteen hydrogen-bonded imino protons, characteristic of GQ structures, show an upfield shift in the region between δ 10.5 and 12 ppm.[48,49] A 1D ^{1}H NMR spectrum of SL15P recorded in Li-cacodylate buffer (pH 7) in the absence of K^+ ions shows imino resonances exclusively in the Watson-Crick region, indicating the formation of an Hp structure (Figure 3C). Upon addition of 2 molar equivalents of KCl in the same buffer, additional resonances appear in the Hoogsteen region, consistent with the formation of an rGQ structure. However, Hp remains the predominant structure, giving an approximate population ratio of rGQ:Hp ≈ 1:4 (Figures 3D, S6 A). Moving to 10 mM KH_2PO_4/K_2HPO_4 (pH 7) buffer with 10 mM KCl rGQ, the rGQ structure becomes the predominant species, yielding an approximate ratio of rGQ:Hp ≈ 3:1 (Figures 3E, S6 B). To obtain rGQ as a single structure in solution, it is necessary to mutate the sequence by replacing the C in position 15 with U (SL15PU15, Figure 3F). Therefore, SL15P can assume an Hp or rGQ structure for which the equilibrium depends on the potassium concentration in solution. The rGQ imino region shows 12 well-resolved resonances, consistent with the presence of three G-quartets. The corresponding CD spectrum (Figure S9) displays a profile characteristic of a parallel rGQ topology. Based on the observed quartet pattern and the fact that the second and third G-tracts are separated by 11 nucleotides, we propose the presence of a long loop connecting G11 and G23, as illustrated in the structural model in Figure 3B.

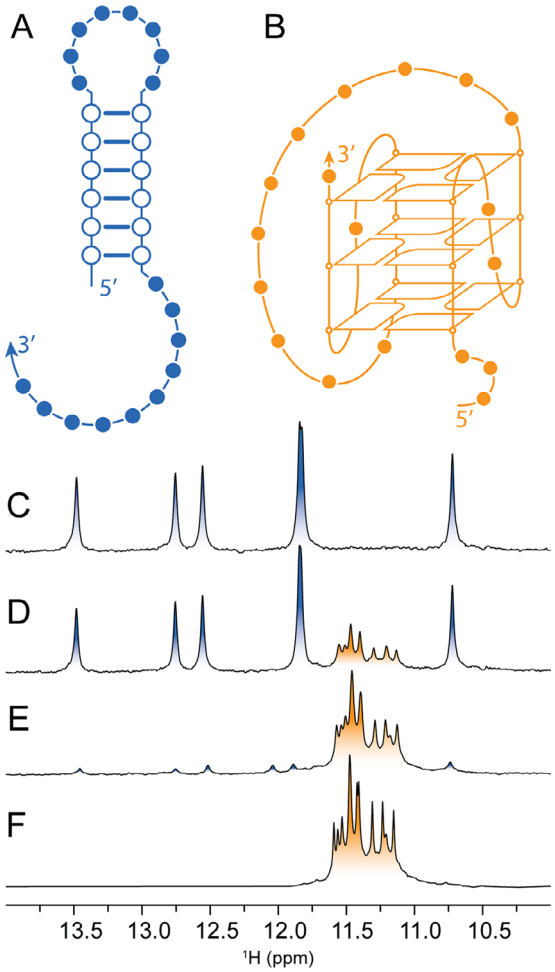

Figure 3. Imino–proton NMR characterization of the SL15P RNA Hp–GQ equilibrium (ongoing studies on resonance assignment): A) Hairpin (Hp) structural model, B) rGQ structural model. (C–F) Imino regions of the 1D ^{1}H NMR spectra recorded at 25 °C under different buffer conditions with Hp peaks in blue and rGQ peaks in orange: C) 10 mM Li–cacodylate (pH = 7) buffer, D) 10 mM Li-cacodylate (pH = 7) buffer and 0.2 mM KCl (rGQ:Hp ≈ 1:4), E) 10 mM KH_2PO_4/K_2HPO_4 (pH = 7) buffer and 10 mM KCl (rGQ:Hp ≈ 3:1), F) C15U mutant (SL15PU15) in 10 mM KH_2PO_4/K_2HPO_4 (pH = 7) buffer and 10 mM KCl.

2.2. NMR Titration Analysis of Small Molecule-Induced Structural Transitions

The imino region is highly informative for assessing interactions between GQs and small molecules.[50,51] In this region, complex formation can be detected by the appearance of new imino peaks. As signals here are typically better resolved than in other spectral regions, structural changes induced by ligand binding can be monitored more easily. The aromatic region of the ^{1}H NMR spectrum (6–9 ppm) provides relevant information regarding interactions between the ligand and nucleobases that are not involved in Hoogsteen or Watson-Crick base pairing and therefore do not exhibit resonances in the imino region. These interactions can occur, for instance, with bases located in the loops of the GQ. However, extensive signal overlap often complicates analysis without the aid of 2D techniques. For this screening, we primarily focused on the imino region, but the

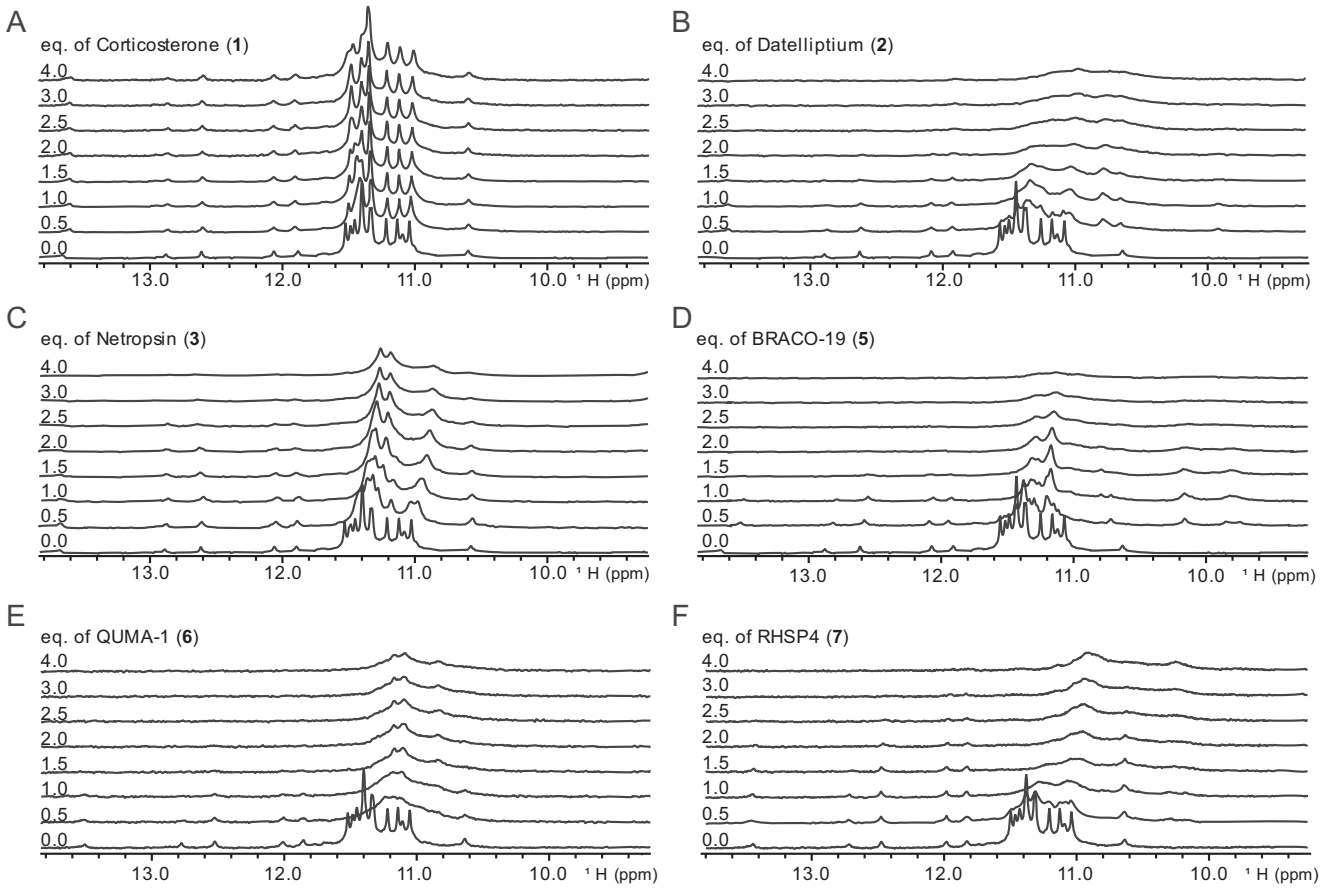

Figure 4. Titration series of SL15P rGQ with weak/noninteracting compounds. All titrations were performed on samples containing 0.1 mM RNA in 10 mM potassium phosphate buffer, 10 mM KCl, and 5% D_2O, at 25 °C, using a 600 MHz NMR spectrometer. Ligands were titrated in steps of 0.5 molar equivalents from 0.5 to 3.0 and in 1.0 molar equivalents from 3.0 to 4.0: A) Corticosterone (1), B) Datelliptium (2), C) Netropsin (3), D) BRACO-19 (5), E) QUMA-1 (6), and F) RHSP4 (7).

aromatic region is reported in Supporting Information (Figure S7). The first step was the titration of each ligand on the SL15P rGQ, conducted at 25 °C in 10 mM KH_2PO_4/K_2HPO_4 buffer (pH 7.0) containing 10 mM KCl, with an rGQ:ligand ratio of approximately 3:1. 1D ^{1}H NMR spectra were acquired after each incremental addition of ligand, with concentrations ranging from 0.5 to 4.0 molar equivalents. Tested ligands displayed distinct behaviors and were therefore grouped according to the resolution of the induced peaks. Some compounds induced only minor changes or caused broadening of the imino resonances, consistent with the presence of multiple species in equilibrium, intermediate exchange processes, or aggregation phenomena, rather than the formation of a well-defined complex. Titration of SL15P with corticosterone (**1**) and netropsin (**3**) has a small impact on the rGQ. For corticosterone (**1**) (Figure 4A), the imino proton resonances remained completely unperturbed, as well as in the aromatic region (Figure S7A), revealing no evidence of interaction between corticosterone (**1**) and the rGQ. While no new resonances appeared, for netropsin (**3**), a more pronounced broadening effect was observed, indicating a weak or nonspecific interaction. Given its known groove-binding properties, netropsin (**3**) may be interacting with other regions of the rGQ, such as the loops, which could indirectly affect the imino resonances. However, analysis of the aromatic region (Figure S7 C) did not provide further structural insights due to excessive signal broadening. Datelliptium (**2**), BRACO-19 (**5**), QUMA-1 (**6**), and RHSP4 (**7**) exhibited comparable effects (Figure 4B,D–F), primarily causing broadening or flattening of the imino resonances upon addition of 0.5 molar equivalents, without the appearance of new signals. Additionally, DOSY spectra (Figure S8) do not show any evidence that would be indicative of complex formation. Both Synucleozide (**4**) and SOP1812 (**8**) showed evidence of interaction with the rGQ structure confirmed by the appearance of new sets of resonances (highlighted in green, Figure 5). However, the significant signal broadening suggests the absence of a single, well-defined specie in solution, which precludes any specific structural information. Specifically, Synucleozide (**4**) induced the appearance of three new imino-proton resonances in the region between δ 10.3 and δ 10.5 ppm, along with an additional broad signal around δ 11.0 ppm. Upon the addition of 0.5 molar equivalents, the native rGQ imino proton resonances show significant broadening. New signals were not observed until 2.5 equivalents had been added, consistent with a fast-exchange regime on the NMR timescale. This behavior suggests a weak interaction, requiring relatively high ligand concentrations to shift the equilibrium toward the rGQ-ligand complex and allowing its observation by NMR. SOP1812 (**8**) (Figure 5B) showed higher selectivity for the rGQ over the

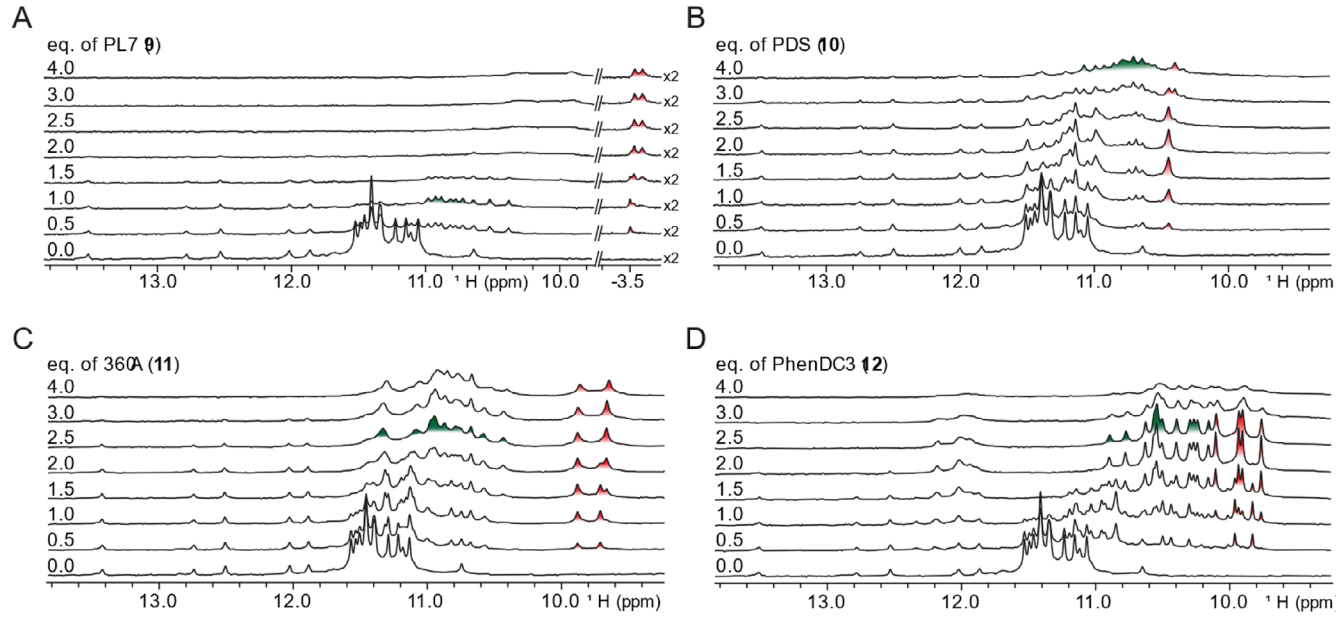

Figure 5. Titration series of SL15P rGQ with high-interaction ligands that exhibit well-defined complex resonances. All titrations were performed on samples containing 0.1 mM RNA in 10 mM potassium phosphate buffer, 10 mM KCl, and 5% D_2O, at 25 °C, using a 600 MHz NMR spectrometer. Ligands were titrated in steps of 0.5 molar equivalents from 0.5 to 3.0 and in 1.0 molar equivalents from 3.0 to 4.0. New resonances of rGQ appearing during the titration are colored green, and the resonances of the bound ligand are colored red: A) PL7 (9), B) PDS (10), C) 360A (11), and D) PhenDC3 (12).

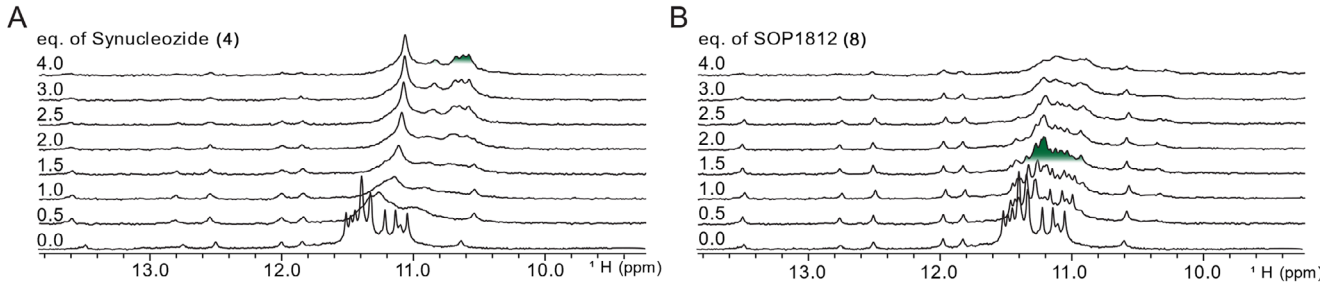

Figure 6. Titration series of SL15P rGQ with interacting ligands that exhibit broadened complex signals. All titrations were performed on samples containing 0.1 mM RNA in 10 mM potassium phosphate buffer, 10 mM KCl, and 5% D_2O, at 25 °C, using a 600 MHz NMR spectrometer. Ligands were titrated in steps of 0.5 molar equivalents from 0.5 to 3.0 and in 1.0 molar equivalents from 3.0 to 4.0. New resonances of rGQ appearing during the titration are colored green: A) Synucleozide (4) and B) SOP1812 (8).

Hp structure. This was evidenced by specific perturbations of the rGQ imino resonances, while the Hp signals remain unaffected even upon addition of 4 molar ligand equivalents. Only minor chemical shift changes were observed in the rGQ imino region, with most resonances retaining their original positions. Furthermore, upon addition of 2.0 molar equivalents of SOP1812 (**8**), imino resonances did not exhibit any further chemical shift changes but instead showed progressive signal broadening and intensity decreasing, indicative of a saturation point.

Four out of the twelve small molecules selected for this screening showed clear evidence of complex formation, as indicated by the appearance of distinct new sets of imino resonances (colored in green in Figure 6) and ligand signals in their bound state (colored in red in Figure 6). PL7 (**9**), a porphyrin derivative, exhibited high binding ability toward the rGQ, as evidenced by the exclusive presence of well-defined and countable complex imino resonances upon addition of 1.0 molar equivalent (Figure 6A). Titration data suggest a 1:1 binding stoichiometry. This is evidenced by the fact that the set of new signals, already present at a 1:1 molar ratio, doesn't show further chemical shift changes upon subsequent ligand addition. These resonances remain stable until the addition of 1.5 ligand equivalents, at which point precipitation is observed in the NMR tube. Further confirmation of complex formation comes from the emergence of new resonances at δ -3.5 ppm, attributable to the inner NH protons of the porphyrin core. Such signals are absent in aqueous solution due to rapid proton exchange phenomena with the solvent. However, they can be observed only upon formation of the PL7(**9**)-rGQ complex. Their appearance suggests that the corresponding protons become less exposed to the solvent, which suppresses their exchange rate.[40] All three GQ ligands, PDS (**10**), 360A (**11**), and PhenDC3 (**12**), exhibited resonances consistent with a slow-exchange regime on the NMR timescale. In the case of PDS (**10**), a new set of imino resonances attributable to the complex appeared only after the addition of 3.0 molar equivalents (Figure 6B). Additionally, PDS (**10**) displayed a

signal that progressively increased around δ 10.2 ppm. Following the addition of 2.5 molar equivalents, a new signal emerged next to the one mentioned before. This indicates that the chemical environment of the ligand proton gradually changes with increasing ligand equivalents, resulting in a slight downfield shift of its NMR resonance. For 360A (**11**) (Figure 6C), the addition of just 0.5 molar equivalents resulted in the appearance of a new set of imino resonances in a slow exchange regime with native ones. Upon the addition of 1.5 molar equivalents, the native rGQ resonances progressively disappeared, suggesting the complex became the predominant specie in solution. Confirmation of complex formation is also provided by the ligand's NMR resonances. For instance, while the symmetric, unbound 360A (**11**) molecule is expected to display a single resonance at δ 9.6 ppm for its two equivalent *ortho* protons to the quinolinium nitrogen (Figure S2), the ROESY spectrum of the 1:1 360A:SL15P complex displays two distinct resonances exhibiting an ROE correlation in a slow-exchange regime on the NMR timescale (Figure S3A). This magnetic nonequivalence indicates a loss of molecular symmetry upon binding to a nonsymmetrical target. Furthermore, upon the addition of 1.5 molar equivalents of 360A, a new signal appears near the one at δ 9.6 ppm. The downfield shift observed in one of the two resonances suggests that only one quinolinium moiety experiences an additional perturbation, potentially due to a structural rearrangement such as the approach or displacement of a nucleobase or a second ligand molecule. The complete disappearance of the free ligand resonances supports the formation of a stable complex. PhenDC3 (**12**) induces an immediate and pronounced perturbation of the rGQ imino resonances upon the addition of 0.5 molar equivalent. This is followed by the progressive emergence of multiple new sets of imino signals, with resonance intensities exceeding those of the native rGQ peaks as the concentration of PhenDC3 (**12**) increase (Figure 6D). These findings support the hypothesis that the phenanthroline scaffold may promote a structural rearrangement of the Hp present in solution into a ligand-stabilized rGQ structure. Furthermore, PhenDC3 (**12**) exhibits two distinct sets of ligand-bound proton resonances, with chemical shifts similar to those observed for 360A (**11**). Also in this case, the *ortho* proton to the quinoline quaternary nitrogen (Figure S4) shows an initial splitting of its signal upon binding, due to a loss of molecular symmetry. As more ligand is added, the two initial resonances shift, and an additional pair emerges, indicating the presence of at least two different binding modes. The ROESY spectrum reveals two cross-peaks that correlate these resonances, one for each pair (Figure S5), supporting the presence of two molecules bound to the rGQ. These molecules exhibit an intramolecular fast exchange regime but not an intermolecular one. These observations suggest that, in addition to the initial symmetry loss, a second binding site on the rGQ may be involved, consistent with the formation of a 1:2 SL15P:PhenDC3.

2.3. Ligand Selectivity and rGQ Refolding

Ligands showing clear NMR evidence of complex formation were selected to investigate their selectivity for rGQ structures and their ability to promote GQ folding. To this end, selected compounds were evaluated under low K^+ conditions, enabling a direct assessment of their influence on the structural equilibrium between the Hp and rGQ structures. As shown in Figure 3, the SL15P oligonucleotide was folded in a 10 mM Li-cacodylate buffer solution in the presence of 0.2 mM of KCl (Figure S6), in which conditions the Hp structure is favored. Each ligand was added at 1 molar equivalent, an average concentration that titrations have previously shown to induce complex formation without triggering precipitation or aggregation. The ligand effect on the SL15P sequence was monitored by acquiring ^{1}H NMR spectra both immediately after ligand addition and again after a thermal annealing cycle (90 °C for 5 minutes, followed by gradual cooling to room temperature over 1 hour). This annealing step was performed to investigate the ligand's ability to function as a molecular template, specifically to determine if it could induce the formation of an rGQ from a single strand that would otherwise spontaneously refold into a Hp structure. In all cases, ligand addition exclusively affected resonances between δ 11.6 and 10.8 ppm, confirming ligands' selectivity for the rGQ structure over the Hp. During the titration, the intensity of the Hp resonances gradually decreases. However, the Hp signals remain sharp, and their chemical shifts do not change, indicating that the ligands do not interact directly with the Hp structure. If such an interaction occurred, signal broadening would be expected. The five ligands exhibited distinct effects on the rGQ structure. SOP1812 (**8**) induced broadening of the native rGQ resonances without the appearance of a new set (Figure 7A). In contrast, PL7 (**9**) caused a complete disappearance of the rGQ resonances, suggesting a tendency to form aggregates (Figure 7B). Both PDS (**10**) and 360A (**11**) induced the emergence of new resonances indicative of the formation of a new complex species, whose intensities increased after thermal annealing (Figure 7C, D). The most pronounced effect was observed with PhenDC3 (**12**) (Figure 7E). Upon its addition, the intensity of the imino Hp signals decreases by approximately half, while new, well-defined peaks emerge. These newly formed resonances display a marked upfield shift, characteristic of rGQ-ligand quartet stacking. Subsequent annealing further increases the number and intensity of resonances, indicating that heat treatment promotes RNA folding into a more defined secondary structure and shifts the equilibrium toward a stabilized rGQ. As a consequence of the thermal treatment, ligand binding becomes more efficient, resulting in improved signal resolution and the appearance of additional ones. These observations, consistent with the titration data, suggest that the formation of the rGQ-ligand complex may involve one or more well-defined intermediate states.

2.4. CD Melting Analysis of SL15PU15-Ligand Complexes

To determine the ligands' ability to stabilize the rGQ structure, we performed thermal melting experiments using CD spectroscopy. CD spectra offer valuable information about potential ligand-induced changes in rGQ topology.[52] To minimize contributions from alternative structures such as the Hp, the mutant oligonucleotide SL15PU15 was employed in this part of the study.

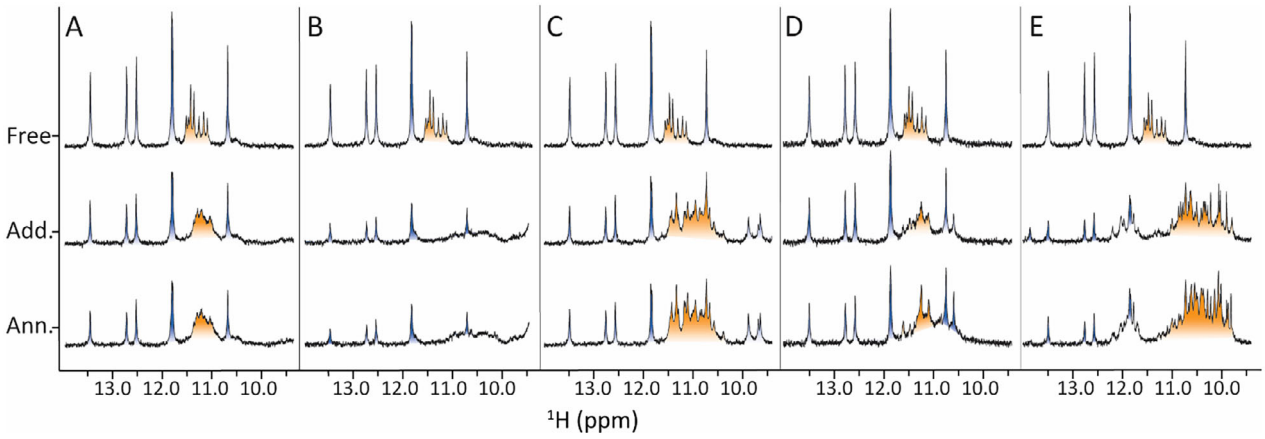

Figure 7. Evaluation of ligand-induced structural modulation under Hp-favoring conditions. All titrations were performed on samples containing 0.1 mM RNA in 10 mM Li-cacodylate (pH = 7) buffer, 0.2 mM of KCl, 5% D_2O, at 25 °C, using a 600 MHz NMR spectrometer. Imino peaks are colored in blue for the Hp and orange for the rGQ structure. Spectra were acquired before (Free) and after the addition of 1 molar equivalent of each ligand (Add.) and subsequently following a thermal annealing step (5 minutes at 90 °C followed by slow cooling) (Ann.): A) SOP1812 (**8**), B) PL7 (**9**), C) PDS (**10**), D) 360A (**11**), and E) PhenDC3 (**12**).

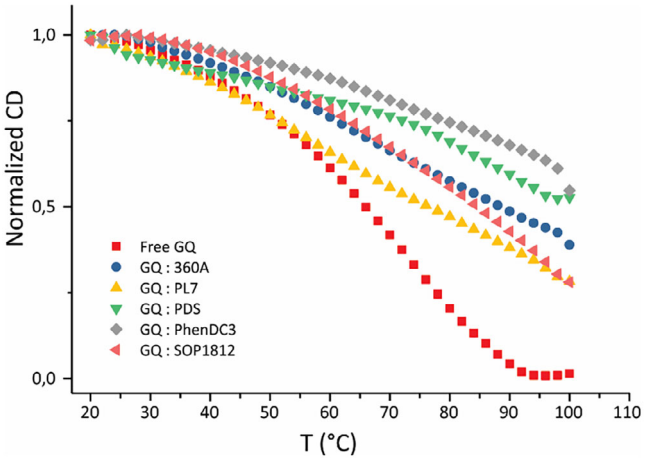

Figure 8. CD melting curves of SL15PU15 GQ, monitored by ellipticity changes at 264 nm as a function of temperature, in the absence and presence of selected small–molecule ligands (1:2 SL15PU15:Ligand molar ratio).

The free SL15PU15 rGQ adopts a parallel topology, as confirmed by a CD profile with a positive maximum at 260 nm and a negative minimum at 240 nm (Figure S9A). Melting experiments were carried out on 20 µM samples of SL15PU15 in a temperature range of 20–100 °C, both in the absence and presence of ligands. In its free state, the rGQ showed a clear melting transition with a T_m of 65.8 °C. None of the tested ligands allowed complete unfolding of the complex, as evidenced by the absence of plateaus in the CD melting curves (Figures 8, S9B-F). As a result, only approximate ΔT_m values could be estimated. Notably, none of the ligands altered the rGQ topology, as CD spectra remained consistent with a parallel fold. PL7 (**9**) and SOP1812 (**8**) showed the weakest stabilizing effects, with an estimated ΔT_m value of approximately ~10 °C. 360A (**11**) significantly enhanced rGQ thermal stability, with a ΔT_m exceeding ~20 °C contributing to a strong stabilization. PDS (**10**) and PhenDC3 (**12**) exhibited the strongest stabilizing effect, increasing the T_m by more than 30 °C approximately. Overall, the thermal stabilization data corroborates the NMR findings on complex formation.

3. Conclusion

The interactions between ligands and rGQs are poorly understood compared to their DNA counterparts. To address this gap, we evaluated a small library of known dGQ stabilizers for their ability to bind to a parallel rGQ formed by the lncRNA-derived sequence, SL15P. The investigation was carried out through NMR titrations to assess complex formation and ligands' ability to promote rGQ folding. Additionally, ligand-induced stabilization was evaluated via CD spectroscopy. The results revealed that many ligands selective for dGQs do not necessarily bind to rGQs with comparable specificity. Notably, several ligands known for their high selectivity and strong stabilizing effects on dGQs failed to form well-defined complexes with the SL15P rGQ studied in this work, resulting in NMR resonance broadening. Among the 12 ligands tested, only six, Synucleozide (**4**), SOP1812 (**8**), PL7 (**9**), PDS (**10**), 360A (**11**), and PhenDC3 (**12**), displayed new sets of NMR resonances consistent with complex formation. For four of these ligands, signals corresponding to the ligand in its bound state were also identified. PL7 (**9**) exhibited resonances at negative chemical shifts (δ –3.5 ppm), corresponding to inner core protons that are typically not observable in aqueous solution. Their detection suggests protection from solvent exchange, likely due to stacking interactions with the G-quartets of rGQ. Additionally, PDS (**10**), 360A (**11**), and PhenDC3 (**12**) exhibited downfield-shifted ligand signals compared to their free forms, while resonances of rGQ were shifted upfield, further confirming complex formation. Our analysis uncovered distinct binding modes. PDS (**10**) maintains its molecular symmetry throughout the titration, suggesting a type of interaction that does not induce significant structural effects. In contrast, the formation of a 1:1 complex between 360A (**11**) and SL15P rGQ is characterized by an immediate loss of ligand structural symmetry followed by an

additional downfield shift of one of the ligand's resonances. This suggests that the local environment around the bound ligand continues to change with an increase of the ligand's concentration, likely due to further structural rearrangements within the complex. Similarly, in the case of PhenDC3 (**12**), the initial interaction with the rGQ causes a loss of ligand structural symmetry. Upon addition of higher molar equivalents, a new set of ligand resonances indicates the binding of a second ligand molecule interacting with the rGQ in a comparable manner but at a different site, supporting the formation of a 1:2 SL15P:ligand complex. Additionally, titration results indicate that while PL7 (**9**), 360A (**11**), and PhenDC3 (**12**) readily promote complex formation with SL15P, shifting the equilibrium toward the rGQ form even at low ligand equivalents, complex formation with PDS (**10**) becomes detectable only after the addition of approximately three molar equivalents. This suggests that PDS has a lower affinity for this specific rGQ, as a substantially higher ligand concentration is required to shift the equilibrium and make the bound state the predominant one in solution. In general, for all these ligands, the upfield imino resonance shifts observed for complex structures are congruent with a predominant stacking interaction mechanism occurring on the G-quartet planes. The same ligands were further evaluated for their ability to promote refolding of SL15P into an rGQ under Hp-favored conditions. Notably, PDS (**10**) and PhenDC3 (**12**) induce the appearance of new resonances corresponding to a ligand-dependent structure. Moreover, both PDS (**10**) and PhenDC3 (**12**) demonstrated the highest stabilizing effect, increasing the melting temperature by over 30 °C. The precise nature of these high-affinity interactions is the subject of ongoing structural studies. From a therapeutic standpoint, a ligand such as PhenDC3 **(12)**, which exhibits strong, specific binding and the ability to induce structural rearrangements in the rGQ, represents a promising candidate as an antagonist able to interfere with rGQ-protein interactions. For these reasons, we believe it is worthwhile pursuing further studies on PhenDC3-SL15P complex to solve their structural details.

Acknowledgments

The authors thank the Slovenian Research and Innovation Agency [ARIS, grants P1-0242 and J1-60019] and the CERIC-ERIC consortium for access to experimental facilities and financial support. G.S. also thanks the CERIC-ERIC consortium for financial support through the DNANANOCERIC project.

Conflict of Interest

The authors declare no conflict of interest.

Data Availability Statement

The datasets and materials supporting the findings of this study are openly available on Zenodo at this link. All relevant data files and documentation have been deposited under a CC–BY 4.0 license and are publicly accessible without embargo.

Keywords: G-quadruplex · ligand · lncrna · NMR spectroscopy

[1] P. Kharel, M. Fay, E. V. Manasova, P. J. Anderson, A. V. Kurkin, J. U. Guo, P. Ivanov, *Nat. Commun.* **2023**, *14*, 205.
[2] S. D. Veenbaas, J. T. Koehn, P. S. Irving, N. N. Lama, K. M. Weeks, *Proc. Natl. Acad. Sci. U.S.A.* **2025**, *122*, e2422346122.
[3] J. Robinson, S. G. Stenspil, K. Maleckaite, M. Bartlett, M. Di Antonio, R. Vilar, M. K. Kuimova, *J. Am. Chem. Soc.* **2024**, *146*, 1009.
[4] D. Varshney, S. M. Cuesta, B. Herdy, U. B. Abdullah, D. Tannahill, S. Balasubramanian, *Sci. Rep.* **2021**, *11*, 22735.
[5] D. Ji, B. Wang, K. W. Lo, C. M. Tsang, C. K. Kwok, *Angew. Chem., Int. Ed.* **2025**, *64*, e202417247.
[6] M. M. Fay, S. M. Lyons, P. Ivanov, *J. Mol. Biol.* **2017**, *429*, 2127.
[7] P. Kharel, N. Bhatter, S. Zubair, S. M. Lyons, P. J. Anderson, P. Ivanov, *Nucl. Acids Res.* **2025**, *53*, gkaf590.
[8] S. Bourdon, P. Herviou, L. Dumas, E. Destefanis, A. Zen, A. Cammas, S. Millevoi, E. Dassi, *Nucl. Acids Res.* **2023**, *51*, D240.
[9] L. Dumas, S. Shin, Q. Rigaud, M. Cargnello, B. Hernández-Suárez, P. Herviou, N. Saint-Laurent, M. Leduc, M. L.e Gall, D. Monchaud, E. Dassi, A. Cammas, S. Millevoi, *Nat. Commun.* **2025**, *16*, 3292.
[10] S. Toden, T. J. Zumwalt, A. Goel, *Biochim. Biophys. Acta* **2021**, *1875*188491.
[11] M. Coan, S. Haefliger, S. Ounzain, R. Johnson, *Nat. Rev. Genet.* **2024**, *25*, 578.
[12] L.-L. Chen, V. N. Kim, *Cell* **2024**, *187*, 6451.
[13] J. S. Mattick, P. P. Amaral, P. Carninci, S. Carpenter, H. Y. Chang, L.-L. Chen, R. Chen, C. Dean, M. E. Dinger, K. A. Fitzgerald, T. R. Gingeras, M. Guttman, T. Hirose, M. Huarte, R. Johnson, C. Kanduri, P. Kapranov, J. B. Lawrence, J. T. Lee, J. T. Mendell, T. R. Mercer, K. J. Moore, S. Nakagawa, J. L. Rinn, D. L. Spector, I. Ulitsky, Y. Wan, J. E. Wilusz, M. Wu, *Nat. Rev. Mol. Cell. Biol.* **2023**, *24*, 430.
[14] C. P. Ponting, P. L. Oliver, W. Reik, *Cell* **2009**, *136*, 629.
[15] P. Agarwala, S. Pandey, S. Maiti, *Org. Biomol. Chem.* **2015**, *13*, 5570.
[16] K. Sato, M. Akiyama, Y. Sakakibara, *Nat. Commun.* **2021**, *12*, 941.
[17] I. Georgakopoulos-Soares, G. E. Parada, M. Hemberg, *Comput. Struct. Biotech. J* **2022**, *20*, 2871.
[18] L. R. Ganser, M. L. Kelly, D. Herschlag, H. M. Al-Hashimi, *Nat. Rev. Mol. Cell. Biol.* **2019**, *20*, 474.
[19] D. Varshney, J. Spiegel, K. Zyner, D. Tannahill, S. Balasubramanian, *Nat. Rev. Mol. Cell. Biol.* **2020**, *21*, 459.
[20] C. Shukla, B. Datta, *Int. J. Biol. Macromol.* **2024**, *278*, 134946.
[21] M. M. Fay, S. M. Lyons, P. Ivanov, *J. Mol. Biol.* **2017**, *429*, 2127.
[22] L. Dumas, P. Herviou, E. Dassi, A. Cammas, S. Millevoi, *Trends Biochem. Sci.* **2021**, *46*, 270.
[23] P. Basu, I. Kejnovská, M. Gajarský, D. Šubert, T. Mikešová, D. Renčiuk, L. Trantírek, J.-L. Mergny, M. Vorlíčková, *Nucl. Acids Res.* **2024**, *52*, 13224 gkae927.
[24] V. J. Sahayasheela, H. Sugiyama, *Cell Chem. Biol.* **2024**, *31*, 53.
[25] A. Ghosh, S. P. Pandey, D. C. Joshi, P. Rana, A. H. Ansari, J. S. Sundar, P. Singh, Y. Khan, M. K. Ekka, D. Chakraborty, S. Maiti, *Nucl. Acids Res.* **2023**, *51*, 9415.
[26] L. Fu, Q. Wu, J. Fu, *Int. J. Biol. Macromol.* **2024**, *268*, 131811.
[27] H. Yari, L. Jin, L. Teng, Y. Wang, Y. Wu, G. Z. Liu, W. Gao, J. Liang, Y. Xi, Y. C. Feng, C. Zhang, Y. Y. Zhang, H. Tabatabaee, T. La, R. H. Yang, F. H. Wang, X. G. Yan, M. Farrelly, R. Scott, T. Liu, R. F. Thorne, S. T. Guo, X. D. Zhang, *Nat. Commun.* **2019**, *10*, 5334.
[28] H. Yari, L. Jin, L. Teng, Y. Wang, Y. Wu, G. Z. Liu, W. Gao, J. Liang, Y. Xi, Y. C. Feng, C. Zhang, Y. Y. Zhang, H. Tabatabaee, T. La, R. H. Yang, F. H. Wang, X. G. Yan, M. Farrelly, R. Scott, T. Liu, R. F. Thorne, S. T. Guo, X. D. Zhang, *Nat. Commun.* **2019**, *10*, 5334.
[29] I. M. A. del Mundo, K. M. Vasquez, G. Wang, *Biochim. Biophys. Acta* **2019**, *1866*, 118539.
[30] T. Santos, G. F. Salgado, E. J. Cabrita, C. Cruz, *Pharm.* **2021**, *14*, 769.
[31] J. Qiu, J. Liu, S. Chen, T.-M. Ou, J.-H. Tan, L.-Q. Gu, Z.-S. Huang, D. Li, *Org. Lett.* **2015**, *17*, 4584.
[32] J. L. Childs-Disney, X. Yang, Q. M. R. Gibaut, Y. Tong, R. T. Batey, M. D. Disney, *Nat. Rev. Drug. Discov.* **2022**, *21*, 736.

[33] A. Randazzo, A. Galeone, V., Esposito, M. Varra, L. Mayol, *Nucleos. Nucleot. Nucl. Ac.* **2002**, *21*, 535.
[34] P. Zhang, H.-J. Park, J. Zhang, E. Junn, R. J. Andrews, S. P. Velagapudi, D. Abegg, K. Vishnu, M. G. Costales, J. L. Childs-Disney, A. Adibekian, W. N. Moss, M. M. Mouradian, M. D. Disney, *Proc. Natl. Acad. Sci. U.S.A.* **2020**, *117*, 1457.
[35] S. M. Gowan, J. R. Harrison, L. Patterson, M. Valenti, M. A. Read, S. Neidle, L. R. Kelland, *Mol. Pharmaceutics* **2002**, *61*, 1154.
[36] S. Neidle, *Mol* **2024**, *29*, 3653.
[37] X. Chen, S. Chen, J. Dai, J. Yuan, T. Ou, Z. Huang, J. Tan, *Angew. Chem., Int. Ed.* **2018**, *57*, 4702.
[38] R. A. Heald, C. Modi, J. C. Cookson, I. Hutchinson, C. A. Laughton, S. M. Gowan, L. R. Kelland, M. F. G. Stevens, *J. Med. Chem.* **2002**, *45*, 590.
[39] A. A. Ahmed, R. Angell, S. Oxenford, J. Worthington, N. Williams, N. Barton, T. G. Fowler, D. E. O'Flynn, M. Sunose, M. McConville, T. Vo, W. D. Wilson, S. A. Karim, J. P. Morton, S. Neidle, *ACS Med. Chem. Lett.* **2020**, *11*, 1634.
[40] G. Satta, M. Trajkovski, A. Cantara, M. Mura, C. Meloni, G. Olla, M. Dobrovolná, L. Pisano, S. Gaspa, A. Salis, L. De Luca, F. Mocci, V. Brazda, J. Plavec, M. Carraro, *Chem. - Eur. J.* **2024**, *30*, e202402600.
[41] G. Pennarun, C. Granotier, L. R. Gauthier, D. Gomez, F. Hoffschir, E. Mandine, J.-F. Riou, J.-L. Mergny, P. Mailliet, F. D. Boussin, *Onc.* **2005**, *24*, 2917.
[42] R. Rodriguez, S. Müller, J. A. Yeoman, C. Trentesaux, J.-F. Riou, S. Balasubramanian, *J. Am. Chem. Soc.* **2008**, *130*, 15758.
[43] A. De Cian, E. DeLemos, J.-L. Mergny, M.-P. Teulade-Fichou, D. Monchaud, *J. Am. Chem. Soc.* **2007**, *129*, 1856.
[44] A. Ghosh, M. Trajkovski, M.-P. Teulade-Fichou, V. Gabelica, J. Plavec, *Angew. Chem., Int. Ed.* **2022**, *61*, e202207384.
[45] S. Roy, A. Ali, S. Bhattacharya, *J. Phys. Chem. B* **2021**, *125*, 5489.
[46] R. Rocca, N. Polerà, G. Juli, K. Grillone, A. Maruca, M. T. Di Martino, A. Artese, J. Amato, B. Pagano, A. Randazzo, P. Tagliaferri, P. Tassone, S. Alcaro, *Arch. Pharm.* **2023**, *356*, 2300134.
[47] M. Garavís, B. López-Méndez, A. Somoza, J. Oyarzabal, C. Dalvit, A. Villasante, R. Campos-Olivas, C. González, *ACS Chem. Biol.* **2014**, *9*, 1559.
[48] M. Adrian, B. Heddi, A. T. Phan, *Methods* **2012**, *57*, 11.
[49] B. Fürtig, C. Richter, J. Wöhnert, H. Schwalbe, *Chem. Bio. Chem.* **2003**, *4*, 936.
[50] S. S. Wijmenga, B. N. M. Van Buuren, *Progr. NMR Spectr.* **1998**, *32*, 287.
[51] J. Plavec, in *Handbook of Chemical Biology of Nucleic Acids* (Ed.: N. Sugimoto), Springer Nature Singapore, Singapore, **2023**, pp. 169–212.
[52] R. del Villar-Guerra, J. O. Trent, J. B. Chaires, *Angew. Chem., Int. Ed.* **2018**, *57*, 7171.

Manuscript received: August 4, 2025
Revised manuscript received: November 5, 2025
Version of record online: November 13, 2025